Spanish-German WE-Heraeus-Seminar
Interdisciplinary Physics of the Sun

How Much Are We Missing? Observational Limits on Magnetic Helicity Transport in Emerging Magnetic Structures

Gwangson Choe,
Sunjung Kim & Sibaek Yi

Department of Astronomy & Space Science
Kyung Hee University, Yongin, Korea

Relative Magnetic Helicity and Helicity Poynting Theorem

actual field in V

potential field in V

H_1 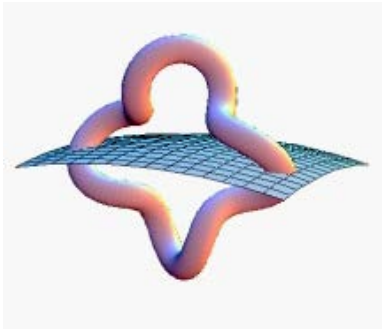 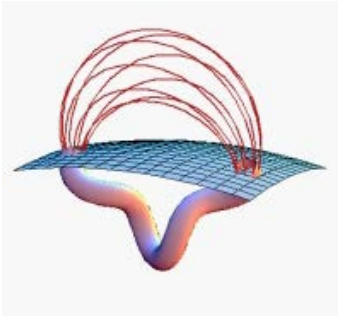 H_0

A gauge invariant form of magnetic helicity in an open volume

$$H \equiv H_1 - H_0 = \int_V \left(\boldsymbol{A} + \boldsymbol{A}_p\right) \cdot \left(\boldsymbol{B} - \boldsymbol{B}_p\right) dV$$

Helicity Poynting theorem

$$\frac{dH}{dt} = 2 \int_S \left[\left(\boldsymbol{A}_p \cdot \boldsymbol{B}_t\right) v_n - \left(\boldsymbol{A}_p \cdot \boldsymbol{v}_t\right) B_n\right] dS$$

where $\hat{n} \cdot \left(\nabla \times \boldsymbol{A}_p\right) = B_n$, $\hat{n} \cdot \boldsymbol{A}_p = 0$, and $\nabla \cdot \boldsymbol{A}_p = 0$.

Démoulin & Berger 2003

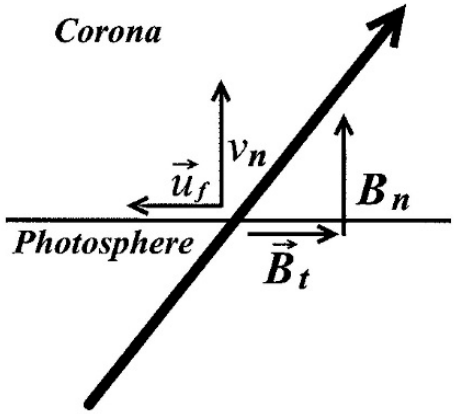

If a flux tube passing through the solar surface pre-exists and if it undergoes a purely vertical motion, its footprint in the photosphere would appear to move horizontally with velocity $\boldsymbol{u_f} = -\frac{v_n}{B_n}\boldsymbol{B}_t$.

If a real horizontal velocity also exists, the footprint in the photosphere would appear to move horizontally with velocity $\boldsymbol{u} = \boldsymbol{v}_t + \boldsymbol{u_f} = \boldsymbol{v}_t - \frac{v_n}{B_n}\boldsymbol{B}_t$.

Then the helicity Poynting theorem simply becomes

$$\frac{dH}{dt} = -2\int_S \left(\boldsymbol{A_p}\cdot\boldsymbol{u}\right)B_n dS.$$

A precise footpoint tracking would be sufficient to obtain the magnetic helicity flux!

But ...

What Happens Where $B_n = 0$?

When a new flux emerges of a pre-existing flux submerges changing the total flux through the photosphere, there is necessarily a place where $B_n = 0$.

Here

$$|\boldsymbol{u}_f| = \left|\left(\frac{v_n}{B_n}\right)\boldsymbol{B}_t\right| \to \infty .$$

but $|B_n \boldsymbol{u}_f| = |v_n \boldsymbol{B}_t|$ remains finite.

Thus, the integral

$$\int_S (\boldsymbol{A_p} \cdot \boldsymbol{u}) B_n dS$$

does not diverge.

However, we cannot detect too small B_n or too large u.

Therefore, there is an observational blackout area near the polarity inversion line.

We Address the Question:

What percentage of the magnetic helicity flux resulting from emergence of a flux rope can be detected?

Assumptions

- Suppose that a flux rope is emerging.
- Assume that a certain area near the PIL is observationally blacked out.
- Outside the blackout area, we assume that the field line footpoints are tracked with infinitely fine spatial and temporal resolution.

Magnetic Helicity of Flux Ropes

We consider infinitely long, axisymmetric flux ropes and compute upper bounds on the helicity influx per unit length along the axial (z-) direction.

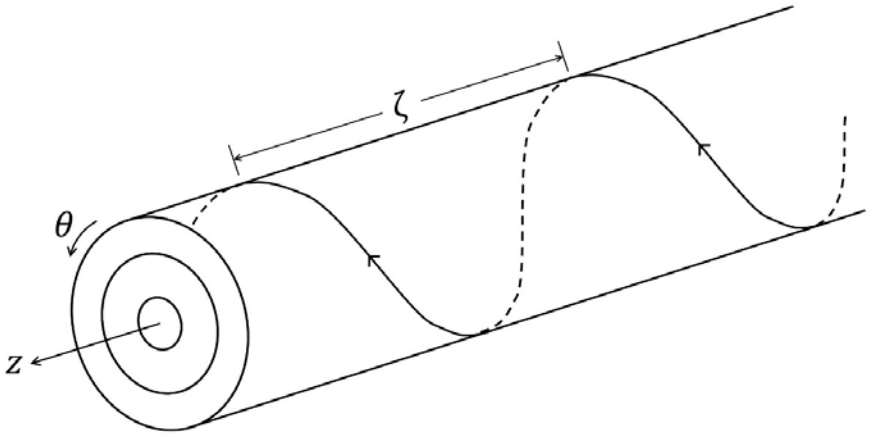

$$H(R) = 2\int_0^R \Phi(r) B_\theta(r)\, dr$$

where

$$\Phi(r) = \int_0^r B_z(r')\, 2\pi r'\, dr'$$

Notations Related to Flux Ropes

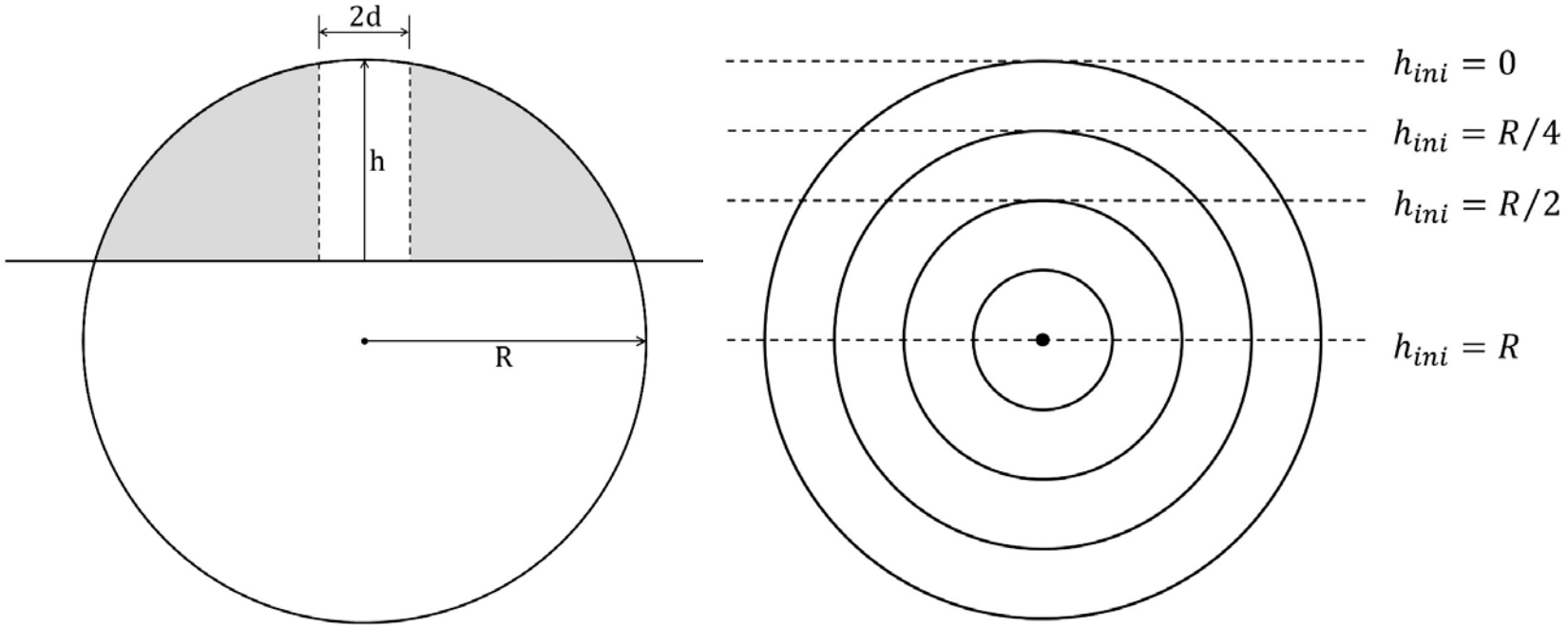

It can be shown that the upper bound of the detectable helicity influx is given by the helicity contained in the shaded region.

Case 1: Gold-Hoyle Flux Rope

- A flux rope, in which all field lines have the same pitch (ζ).
- A non-linear force-free field.

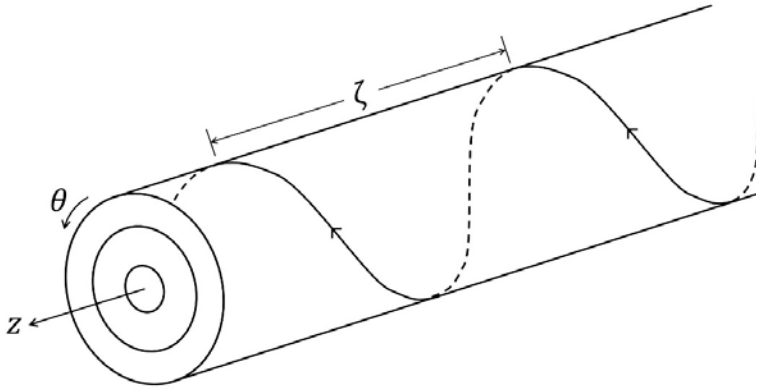

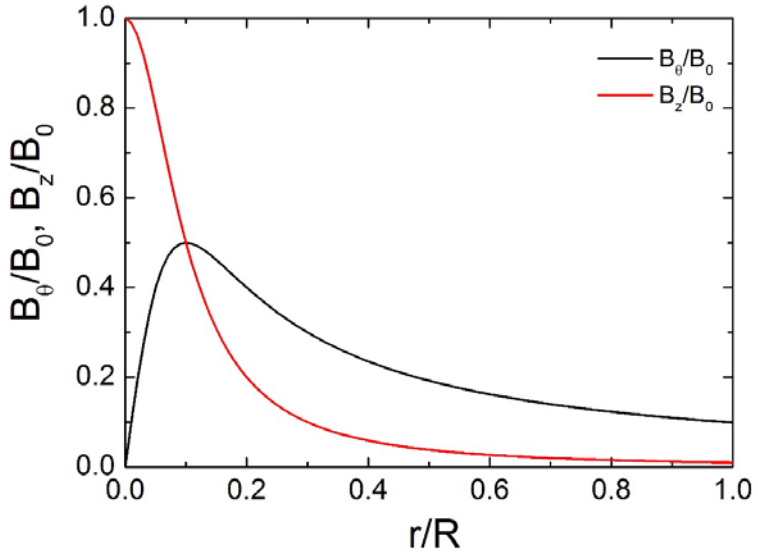

$$H(R) = \nu[\Phi(R)]^2$$

where $\nu = 1/\zeta$, the number of turns per unit length in z

Case 1: Observable Magnetic Flux

poloidal flux

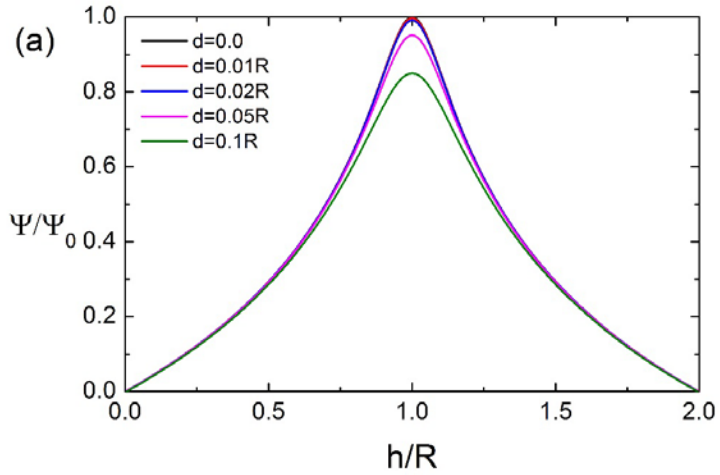

toroidal flux

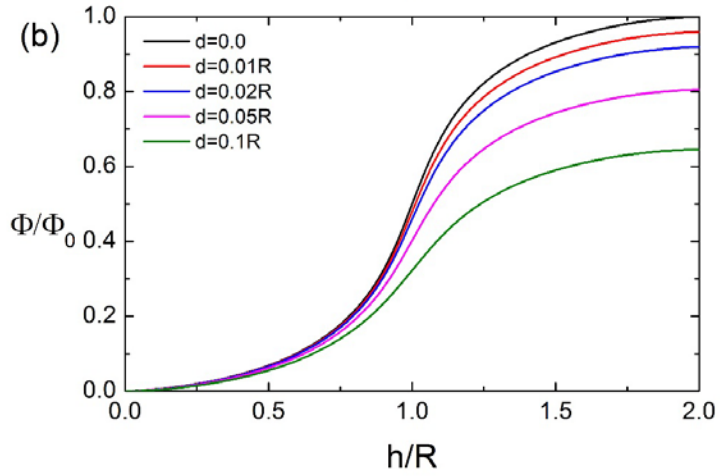

Case 1: Observable Integrated Helicity Flux

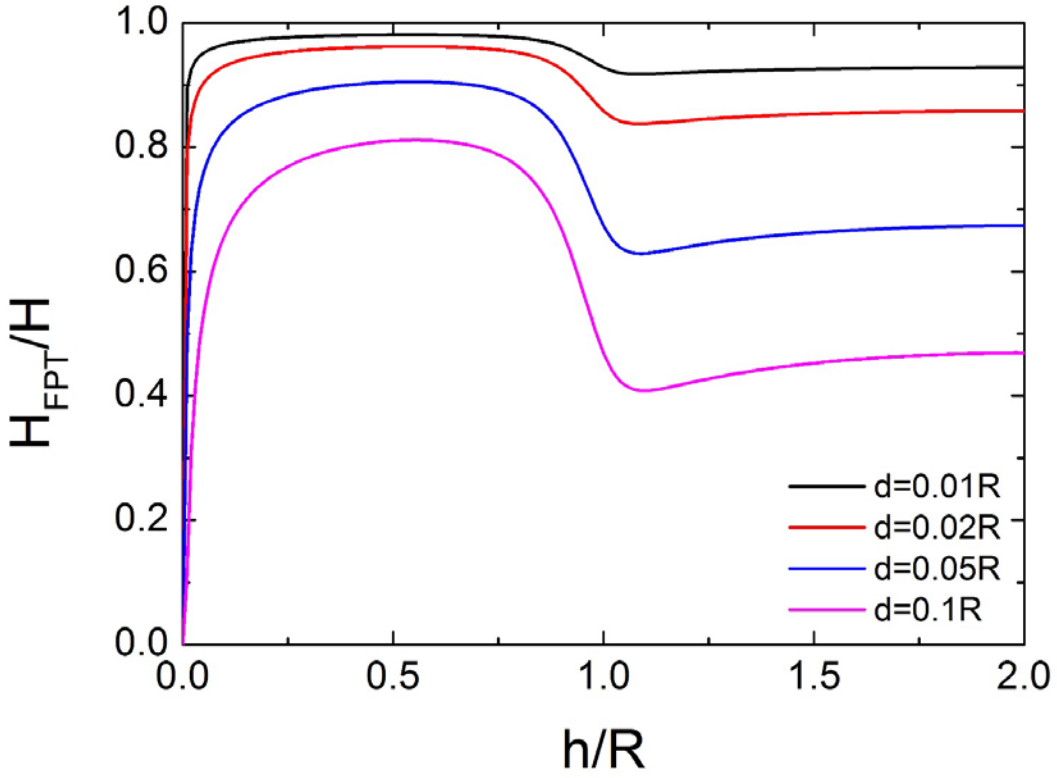

Initially, the flux rope is assumed to be totally under the photosphere.

Case 1: Observable Integrated Helicity Flux for Different Measurement Starting Planes

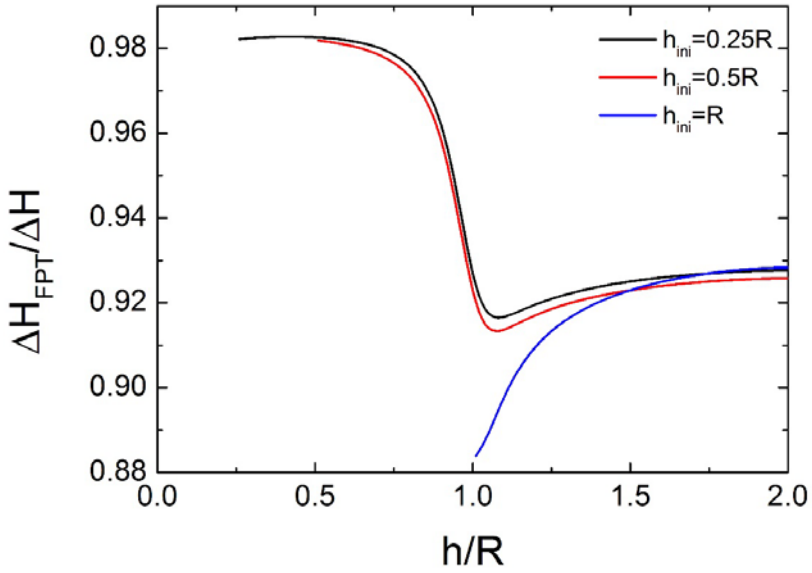

d = 0.01R

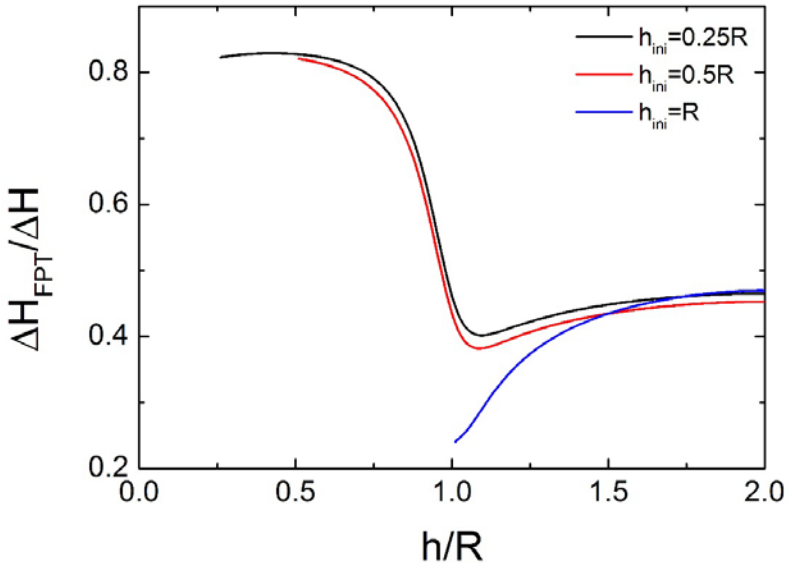

d = 0.1R

Case 2: Lundquist Flux Rope

- A flux rope, which is a linear force-free field satisfying $\nabla \times \boldsymbol{B} = \alpha \boldsymbol{B}$.
- B_z changes sign at $\alpha r \approx 2.405$ and B_θ changes sign at $\alpha r \approx 3.381$.

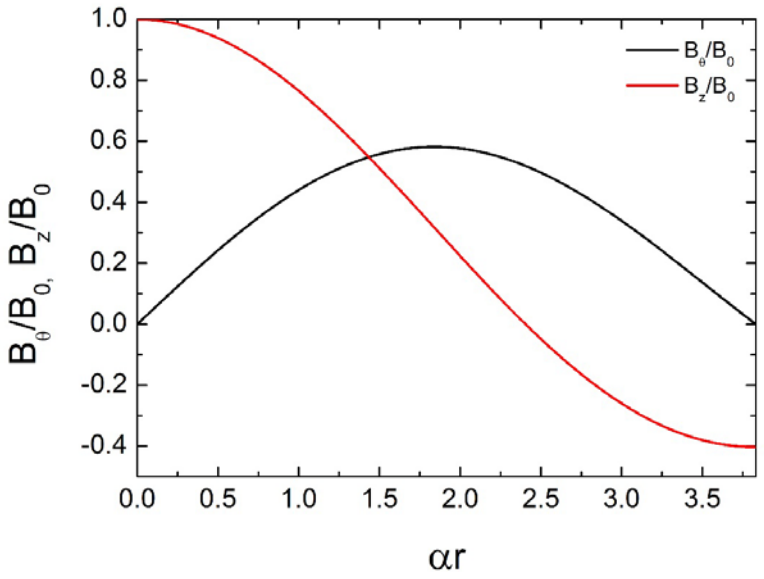

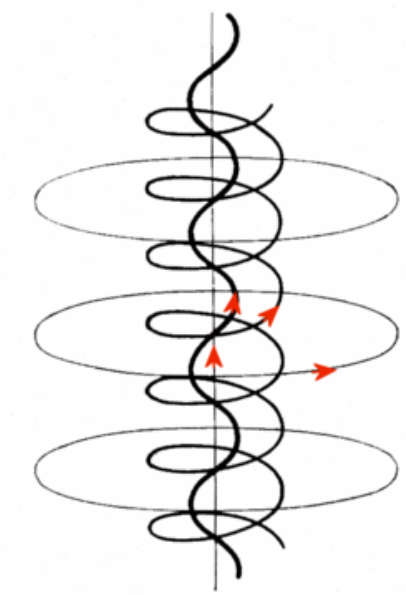

Case 2a: boundary at $\alpha r \approx 2.405$

Case 2b: boundary at $\alpha r \approx 3.381$

Case 2: Observable Magnetic Flux

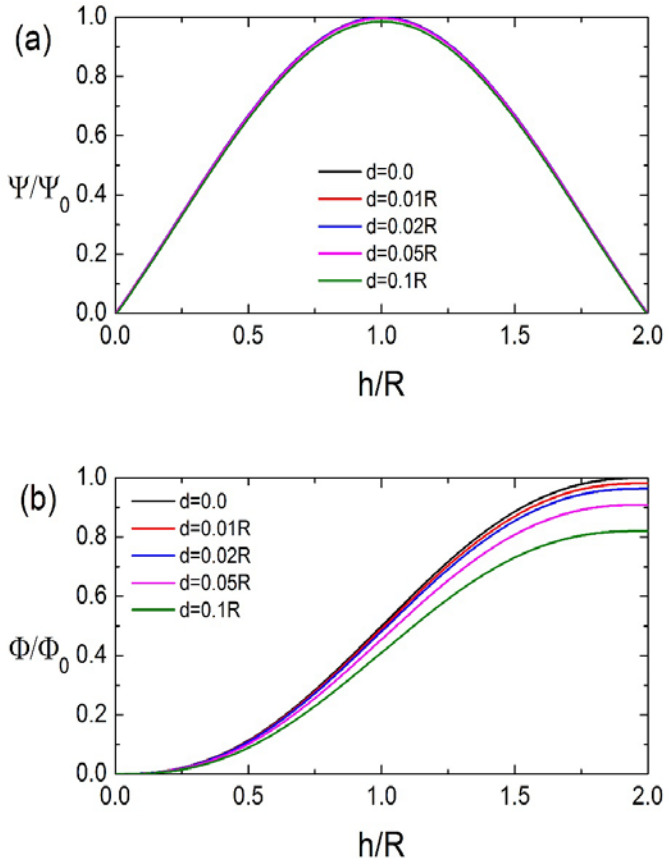

Case 2a

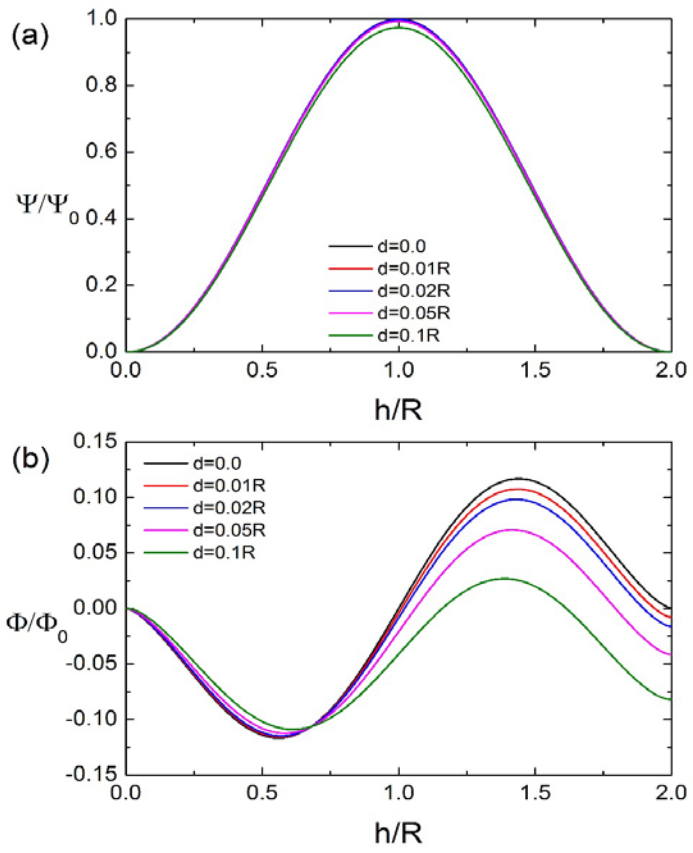

Case 2b

Case 2a: Observable Integrated Helicity Flux

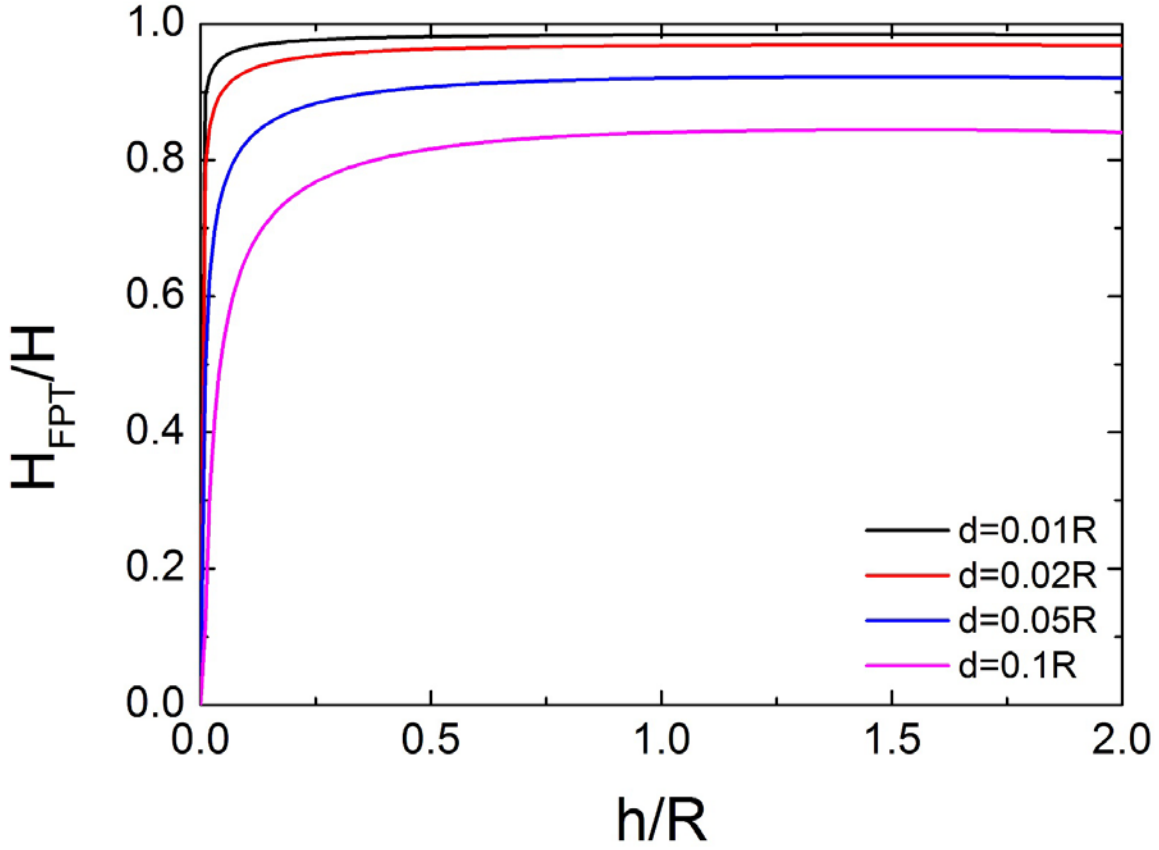

Initially, the flux rope is assumed to be totally under the photosphere.

Case 2a: Observable Integrated Helicity Flux for Different Measurement Starting Planes

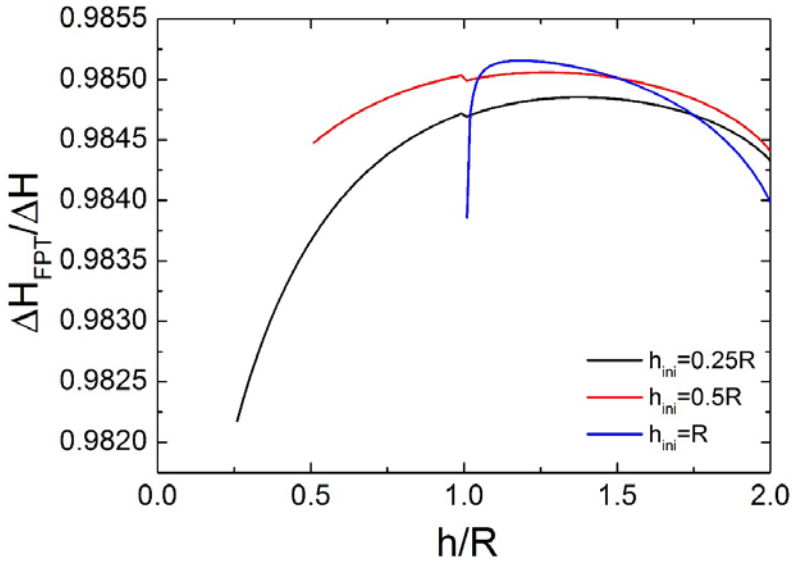

d = 0.01R

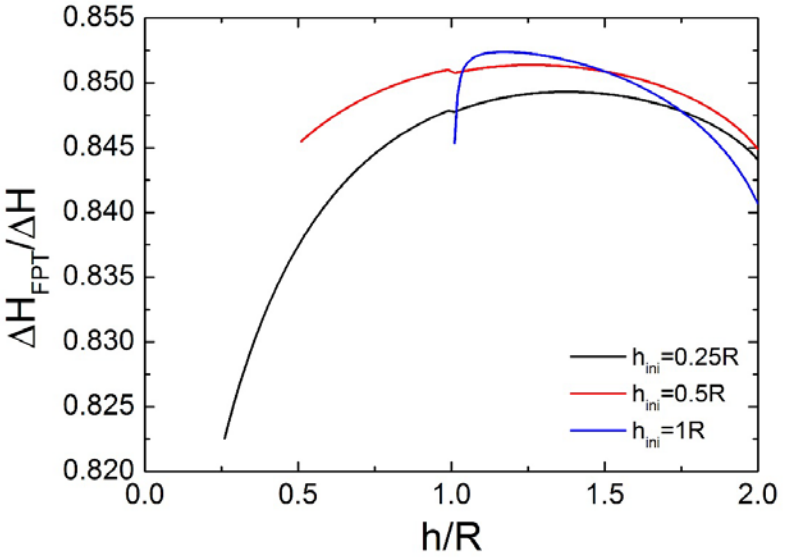

d = 0.1R

Case 2b: Observable Integrated Helicity Flux

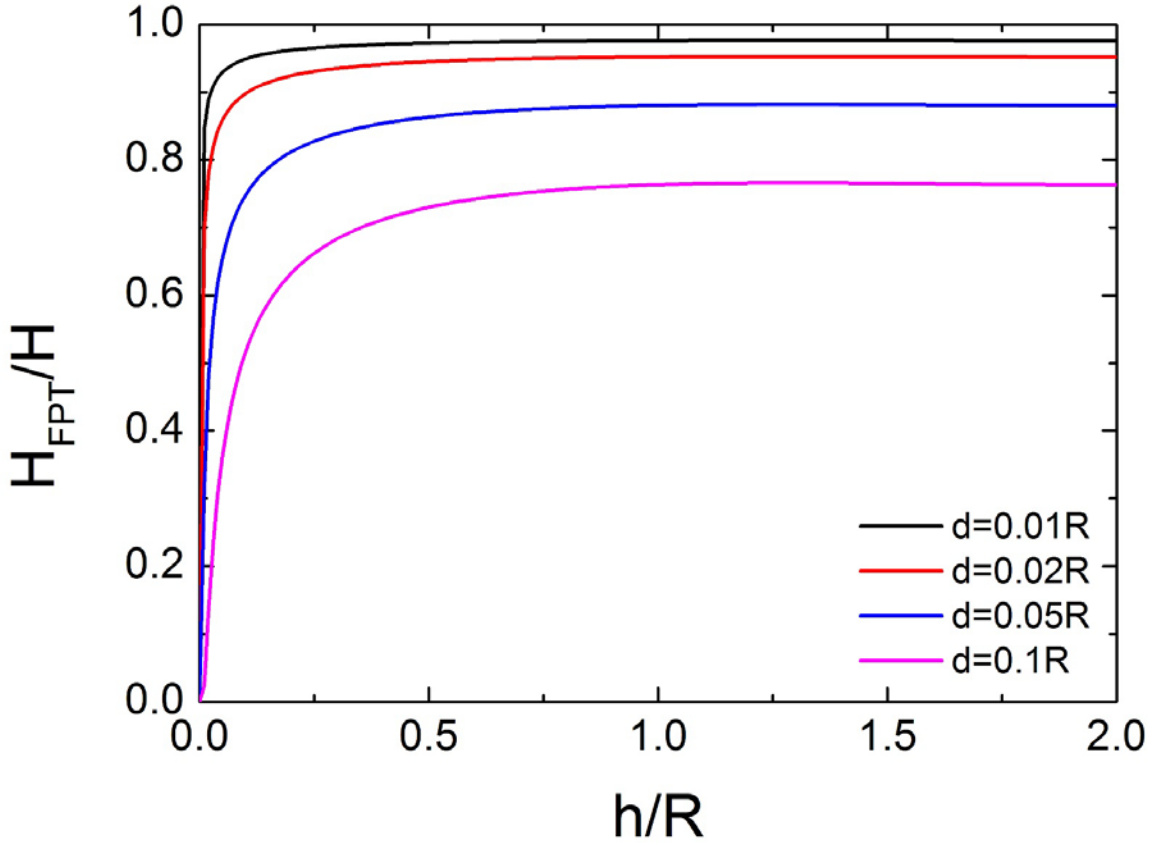

Initially, the flux rope is assumed to be totally under the photosphere.

Case 2b: Observable Integrated Helicity Flux for Different Measurement Starting Planes

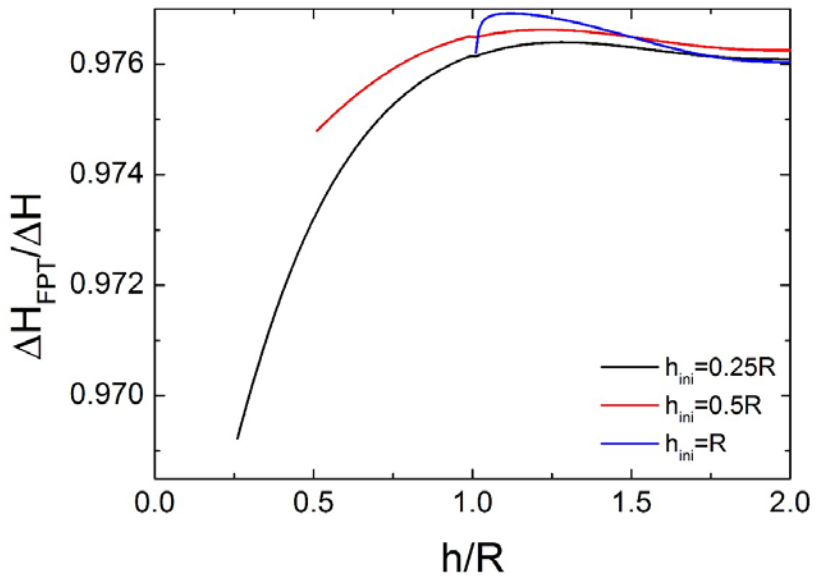

d = 0.01R

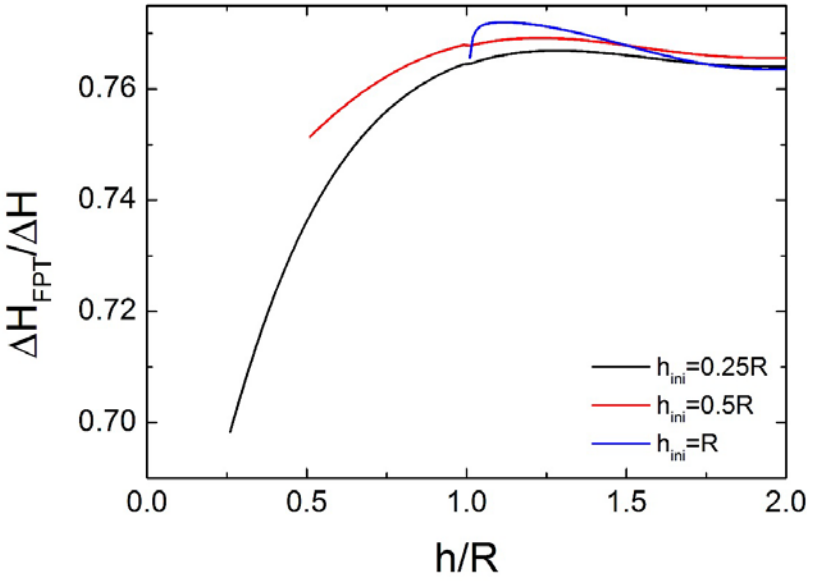

d = 0.1R

Summary

- The magnetic helicity influx estimated by a footpoint tracking method inevitably involves an error due to the blackout area near the polarity inversion line.
- The amount of the error depends on the size of the emerging (submerging) flux region. The smaller the emerging flux region is, the larger is the error incurred.
- Emergence of a Gold-Hoyle flux rope produces larger errors (up to 60%) than that of Lundquist flux ropes. This suggests that the accuracy in the toroidal flux (flux of the field along the PIL) measurement is more important than that in the poloidal flux (flux of the field perpendicular to the PIL) measurement.